Dynamic scaling of the restoration of rotational symmetry in Heisenberg quantum antiferromagnets

Phillip Weinberg and Anders W. Sandvik
Department of Physics, Boston University, 590 Commonwealth Avenue, Boston, Massachusetts 02215, USA
(Received 5 June 2017; published 28 August 2017)

We apply imaginary-time evolution with the operator $e^{-\tau H}$ to study relaxation dynamics of gapless quantum antiferromagnets described by the spin-rotation-invariant Heisenberg Hamiltonian H. Using quantum Monte Carlo simulations to obtain unbiased results, we propagate an initial state with maximal order parameter m_s^z (the staggered magnetization) in the z spin direction and monitor the expectation value $\langle m_s \rangle$ as a function of imaginary time τ. Results for different system sizes (lengths) L exhibit an initial essentially size independent relaxation of $\langle m_s \rangle$ toward its value in the infinite-size spontaneously symmetry broken state, followed by a strongly size dependent final decay to zero when the O(3) rotational symmetry of the order parameter is restored. We develop a generic finite-size scaling theory that shows the relaxation time diverges asymptotically as L^z, where z is the dynamic exponent of the low-energy excitations. We use the scaling theory to develop a practical way of extracting the dynamic exponent from the numerical finite-size data, systematically eliminating scaling corrections. We apply the method to spin-1/2 Heisenberg antiferromagnets on two different lattice geometries: the standard two-dimensional (2D) square lattice and a site-diluted 2D square lattice at the percolation threshold. In the 2D case we obtain $z = 2.001(5)$, which is consistent with the known value $z = 2$, while for the site-diluted lattice we find $z = 3.90(1)$ or $z = 2.056(8)D_f$, where $D_f = 91/48$ is the fractal dimensionality of the percolating system. This is an improvement on previous estimates of $z \approx 3.7$. The scaling results also show a fundamental difference between the two cases; for the 2D square lattice, the data can be collapsed onto a common scaling function even when $\langle m_s \rangle$ is relatively large, reflecting the Anderson tower of quantum rotor states with a common dynamic exponent $z = 2$. For the diluted 2D square lattice, the scaling works well only for small $\langle m_s \rangle$, indicating a mixture of different relaxation-time scalings between the low-energy states. Nevertheless, the low-energy dynamic here also corresponds to a tower of excitations.

DOI: 10.1103/PhysRevB.96.054442

I. INTRODUCTION

Experimental studies of interacting quantum systems are increasingly focusing on nonequilibrium setups, e.g., driving cold-atom systems or electronic materials dynamically through various finite-temperature and quantum phase transitions [1–8]. Theoretical modeling of systems under these conditions is even more challenging than the already difficult problem of computing equilibrium properties of quantum systems away from perturbative regimes. Exact numerical calculations are possible for small systems, and there has been some success in studying issues such as thermalization and many-body localization [9–15]. Reaching system sizes sufficiently large enough for modeling experiments is still difficult in most cases, with the exception of some one-dimensional (1D) systems where the density-matrix renormalization-group (DMRG) method (or the closely related matrix-product states) now allows for time-evolution studies on relatively large system sizes and long times [16–18]. For higher-dimensional systems the challenges in real-time calculations are formidable.

Given the difficulties with real-time evolution, alternative ways to extract nonequilibrium dynamical properties of quantum systems have been explored in the imaginary-time domain, where quantum Monte Carlo (QMC) methods can be applied. In equilibrium, there are solid relationships between real- and imaginary-time correlation functions which can be exploited in numerical analytic continuation of QMC data [19]. Much less is known about practical ways to infer real-time properties from imaginary-time calculations out of equilibrium, although some progress has been made on this front recently. Examples include studies of systems driven through a quantum critical point [20–22] at different velocities or according to nonlinear protocols, where Kibble-Zurek scaling [23–30] can be used to extract the dynamic exponent and other important quantities such as the quantum geometric tensor [20,21,31]. An important observation here is that real- and imaginary-time evolutions not only are identical in the adiabatic limit, where both dynamics keep systems in their instantaneous ground states, but also include the leading nonadiabatic effects. Another example is the phenomenon of "initial slip" [32–36], where a random product state is evolved by a Hamiltonian tuned to a quantum critical point and the state initially becomes increasingly ordered, before developing critical fluctuations and vanishing long-range order. The transient states produced before one reaches the critical equilibrium state have interesting properties that can be probed in imaginary time [32–34]. Imaginary-time evolution has also been used to investigate the emergence of topological conservation laws [37].

In this paper we use the imaginary-time approach to study the relaxation mechanism of the order parameter in quantum antiferromagnets with O(3) rotationally invariant order parameters. The system, described by a Hamiltonian H, is initially prepared in a fully saturated antiferromagnetic state with the order parameter along the z spin axis. Evolving this state in imaginary time τ with the operator $e^{-\tau H}$, the rotational symmetry will eventually be restored, marked by the expectation value of the z component of the order parameter decaying to zero. We identify short- and long-time behavior of the dynamics and develop theoretical and practical tools for analyzing emergent scaling behaviors by defining an effective dynamic exponent for a given threshold value of the z component of the order parameter. As we shall show in this paper, this effective dynamic exponent converges to the dynamic exponent of the *ground state* as the threshold of the order parameter is lowered to zero. In addition to delivering the dynamic exponent of the ground state, which is not very surprising (although useful in its utility as a tool to extract the exponent in many different models which are amenable to QMC methods), we show that the asymptotic long-time, large-system scaling behavior contains valuable information on the nature of the high-energy states. In a clean two-dimensional (2D) Heisenberg antiferromagnet we observe fast convergence of the effective dynamic as the threshold order parameter is decreased, which we argue is indicative of the expected "Anderson tower" of quantum rotor states (states which allow for spontaneous symmetry breaking to form the zero-mode of the spin-wave excitations) [38]. In other words, the scaling is characterized by a constant effective dynamic exponent $z = D$ (D being the dimensionality of the system) for a large range of values of the order parameter. In contrast, in a 2D system randomly diluted at its percolation point, we find that the effective dynamic exponent increases as the threshold order parameter goes to zero, converging toward a fixed value only when the order parameter is small. This demonstrates a hierarchy of excitations which form the tower governed by a common dynamic (size-scaling) exponent only at low energies. The ultimate low-energy value of the dynamic exponent is $z = 3.90(1)$, which improves previous estimates $z \approx 3.7$ obtained using different methods [39–41]. These results reinforce the notion that the lowest excitations of the system at the percolation point are not conventional Anderson quantum rotor states (Goldstone modes [38,42]), although the system breaks the O(3) spin symmetry spontaneously in the thermodynamic limit [43,44].

The outline of the rest of the paper is as follows: In Sec. II we describe the theoretical underpinnings of our approach. In Secs. III and IV we discuss results for the pure 2D Heisenberg model and the diluted system, respectively. We summarize our study and provide some further remarks in Sec. V.

II. RELAXATION AND FINITE-SIZE SCALING

As mentioned in the Introduction, our setup is the following: We prepare our system initially in a fully saturated antiferromagnetic state denoted by $|\psi_0\rangle$ and evolve in imaginary time with $e^{-\tau H}$, where H is a Heisenberg Hamiltonian describing a gapless quantum antiferromagnet. Because the ground state obeys the symmetry of H, we know that this initial state will not be an eigenstate of H, but it will have some overlap with the ground state, as they share the same ordering. As the state evolves in imaginary time, it will eventually decay to the ground state, restoring the rotational symmetry of our system. From the theory of spontaneous symmetry breaking we know that in the limit of system size tending to infinity, a set of excited states just above the rotationally symmetric ground state becomes degenerate, allowing the system to spontaneously align along a particular axis when subjected to an infinitesimal perturbation [42,45]. In imaginary-time this phenomenon will manifest itself as a divergence in the relaxation time to reach the ground state as the system size is increased. We will use the staggered magnetization m_s^z along the z spin axis,

$$m_s^z = \sum_{i_x,i_y} (-1)^{i_x+i_y} S^z_{i_x,i_y}, \tag{1}$$

as a measure of the restoration of rotational symmetry as our state is evolving in imaginary time. The expectation value of this operator as a function of imaginary time is given by

$$\langle m_s^z(\tau)\rangle = \frac{\langle\psi(\tau)|m_s^z|\psi(\tau)\rangle}{\langle\psi(\tau)|\psi(\tau)\rangle}, \tag{2}$$

where $|\psi(\tau)\rangle$ is the imaginary-time evolved state:

$$|\psi(\tau)\rangle = \exp(-\tau H)|\psi(0)\rangle. \tag{3}$$

Expanding in eigenstates of H, denoting the eigenstates and eigenenergies by $|n\rangle$ and ϵ_n, respectively, and defining the gap $\Delta = \epsilon_1 - \epsilon_0$, in the limit $\tau \to \infty$, the expectation value in Eq. (2) will vanish as

$$\langle m_s^z(\tau)\rangle \approx \left(\langle 0|m_s^z|1\rangle \frac{c_1}{c_0} + \text{c.c.}\right) e^{-\Delta\tau} + \cdots, \tag{4}$$

where $c_n = \langle n|\psi_0\rangle$. Since the ground state is symmetric under rotations, we have that $\langle 0|m_s^z|0\rangle = 0$. Let us define the relaxation time τ_r as the time where $\langle m_s^z(\tau)\rangle$ drops below some threshold $m_{\text{threshold}}$. Equation (4) suggests that as this threshold goes to zero, $\tau_r \sim 1/\Delta$. Therefore in this limit, by calculating the scaling τ_r with system size, we can infer the scaling of the low-energy gap of H.

One can characterize this scaling of the low-energy gap by the dynamic exponent $\Delta \sim L^{-z}$, which has different interpretations depending on its value. $z = 0$ implies that the system has a finite gap in the thermodynamic limit, while finite z means the system has gapless excitations, and finally, $z = \infty$ denotes exponential scaling of the gap. If we consider systems which have gapless excitations, a finite dynamic exponent implies the relaxation time should scale as a power law: $\tau_r \sim L^z$. In other words, if one rescales the time axis by L^z, $\langle m_s^z(\tau)\rangle$ should show scaling collapse at small $m_{\text{threshold}}$. For some Hamiltonians there exists a large, but subextensive, number of low-energy states which have energies (relative to the ground state) that have the same scaling as the low-energy gap [38,42]. The existence of these states will have the effect that there will be a larger window of $m_{\text{threshold}}$ for which this scaling collapse holds. This is because higher-order terms in Eq. (4) will have energy exponentials which all scale in a similar manner with system size. This argument will be important later when we discuss the differences between the clean and diluted 2D Heisenberg models in later sections. We would like to clarify that the dynamic exponent in the context models which exhibit spontaneous symmetry breaking of a continuous symmetry is different from the dynamic exponent of the quasiparticle excitations which arise out of the symmetry-broken state [e.g., dynamic exponent associated with quasiparticle dispersion relations of the form $E(k) \sim k^z$] and instead is the dynamic exponent of the states which form the symmetry-broken state.

The preceding arguments, however, become valid asymptotically in the limit $L \to \infty$, and so it is necessary to take into account finite-size corrections if one would like quantitative estimates for the dynamic exponent. As we will explain in the rest of this section, it is possible to control for the effects of finite-size deviations by calculating the "flow" of the dynamic exponent from finite-size systems in a manner similar to the techniques used in finite-size scaling near critical points in equilibrium [46–49]. Using these methods, one can extrapolate the finite-size results to the thermodynamic limit.

To estimate the dynamic exponent from finite-size systems we start by calculating the relaxation times τ_r and τ_r' (at some finite value of $m_{\text{threshold}}$) for two different system sizes L and L', respectively. From this, the dynamic exponent can be estimated by rescaling the two times by their respective system sizes such that the rescaled results are equal:

$$\tau_r L^{z(L,L')} = \tau_r' L'^{z(L,L')}. \tag{5}$$

From this expression we can define a finite-size exponent for the pair of system sizes $z(L,L')$:

$$z(L,L') = \frac{\ln(\tau_r/\tau_r')}{\ln(L/L')}. \tag{6}$$

As $L,L' \to \infty$, this finite-size exponent will converge to what we shall call the effective dynamic exponent (recall that $m_{\text{threshold}}$ is finite), which we denote as z_∞. The manner in which $z(L,L')$ converges to infinite size is determined by corrections to the L^{-z_∞} scaling of $\Delta(L)$. To see this, one can parametrize the corrections to the low-energy gap with correction exponents ω_i:

$$\Delta(L) = L^{-z_\infty}(1 + c_1 L^{-\omega_1} + \cdots). \tag{7}$$

Now modifying Eq. (5) to include corrections, we get

$$\tau_r \Delta(L) = \tau_r' \Delta(L'). \tag{8}$$

Using this equation and Eq. (6), we find that $z(L,L')$ converges to z_∞ as

$$z(L,L') = z_\infty + c_1 \frac{L^{-\omega_1} - L'^{-\omega_1}}{\ln(L'/L)} + \cdots. \tag{9}$$

The equation above allows one to extract both ω_i's and c_i's needed to obtain the scaling corrections in $\Delta(L)$. Note that we have explicitly suppressed the fact that the effective dynamic exponent and the finite-size corrections are functions of $m_{\text{threshold}}$. We will revisit this functional dependence in later sections, but it is important to recall our previous argument that in the limit $m_{\text{threshold}} \to 0$, z_∞ converges to the true dynamic exponent of the model.

In the following we test this scaling hypothesis on two examples. First, we study the Heisenberg antiferromagnetic on the simple square lattice. The low-energy physics of this model is very well understood and provides a good benchmark for our scaling approach [38,45,50,51]. We then go on to apply this method to the site-diluted Heisenberg antiferromagnet on a square lattice at the percolation point, where there have been previous studies but not as clear of a consensus as to the low-energy physics of the model [39–41]. To compute the imaginary-time evolution, we use a projector QMC method that in practice shares many similarities with the common stochastic series expansion (SSE) method. We sample contributions to $\langle\psi_0|H^{2m}|\psi_0\rangle$ and define $\tau = m/N$, where N is the total number of spins on the lattice. This time definition is equivalent, up to a factor, to the conventional imaginary time appearing in the Schrödinger evolution operator [52,53].

III. CLEAN HEISENBERG ANTIFERROMAGNET

For the first example we consider the standard 2D antiferromagnetic Heisenberg model, defined by the Hamiltonian

$$H = J \sum_{\langle i,j \rangle} \mathbf{S}_i \cdot \mathbf{S}_j, \tag{10}$$

where $\mathbf{S}_i$ is a spin-1/2 operator at lattice site i and the sum is over nearest neighbors on an $L \times L$ square lattice in $D = 2$ with periodic boundary conditions. We set $J = 1$ for the rest of the paper. This model is a part of a broad class of antiferromagnet models on translationally invariant bipartite lattices which are known to have quantum-rotor-like low-energy excitations [38]. These excited states have energy levels which become degenerate with the ground state in the limit $L \to \infty$ as a power law: $E_{\text{rotor}} - E_{\text{GS}} \sim L^{-z}$. Here $z = D$ is the dimension of the lattice, and L is the linear dimension of the system. One can think of these quantum rotor states as the quantization of the global angular fluctuations of the order parameter which in the thermodynamic limit form a basis in the ground-state manifold used to create the symmetry-broken ground state which is the vacuum of the gapless spin-wave excitations [45,50,51,54]. Figure 1(a) shows $\langle m_s^z(\tau)\rangle$ versus τ for various system sizes. In this figure we clearly see that, initially, all the system sizes relax at the same rate but then eventually break off from one another when the sublattice magnetization reaches $\langle m_s^z(\tau)\rangle \approx 0.3$, with the larger system sizes taking longer to relax to $\langle m_s^z(\tau)\rangle \to 0$. One may recall that in the ground state of this model the thermodynamic value of $\langle m_s^z(T=0)\rangle \approx 0.307$ [55], which roughly corresponds to the value where the different system sizes begin to relax at different rates (see the dashed line in Fig 1).

One can make use of the continuum-field-theory description of the long-wavelength behavior of this model to understand the evolution of the order parameter in imaginary time. The lowest-energy states of the continuum field theory are uniform in space. Since the initial state is also uniform and the system is translationally invariant, the evolution will occur within the subspace of uniform configurations. The dynamics in this subspace simplify to that of a quantum particle relaxing in the "Mexican-hat" potential. Here the probability distribution of the particle in space represents the probability distribution of the order parameter of the system. Since the initial order parameter value is 0.5, the initial probability distribution of the order parameter is localized away from the minimum of the potential, which for the Heisenberg model on a square lattice is close to 0.3, as illustrated schematically in Fig. 2, panel (i). As the system evolves in imaginary time, the energy of the system decreases, and the order parameter decays until it reaches the bottom of the potential, which in the thermodynamic limit corresponds to the symmetry-broken "ground state," as in Fig. 2, panel (ii). However, because the system is finite, this is not a true ground state, so the energy of the system continues to decay, and the mean magnetization along the z axis relaxes to zero as the probability distribution spreads out over all possible solid angles [Fig. 2, panel (iii)]. This second part of the relaxation is governed by the rotor states as they are the states which make up the quantization of the angular part of

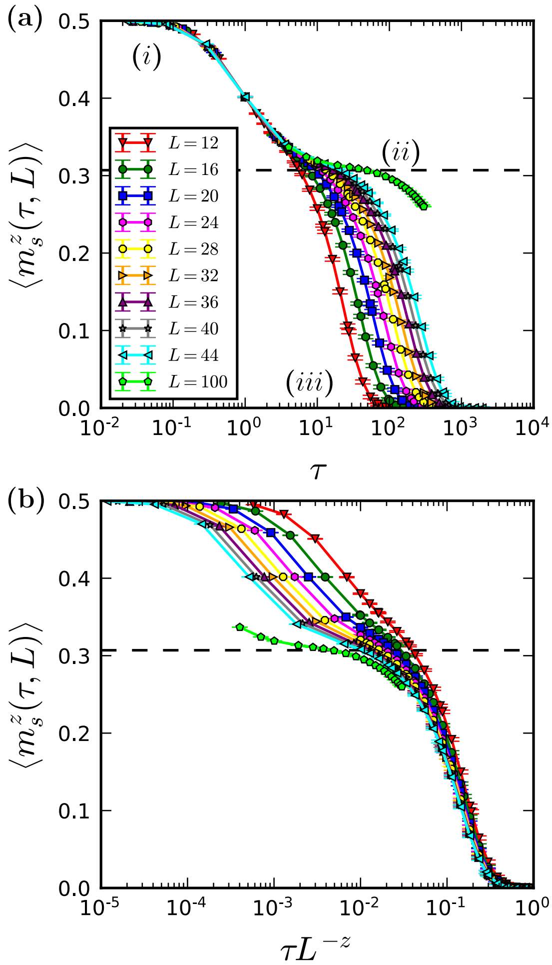

FIG. 1. (a) Evolution of $\langle m_s^z\rangle$ as a function of imaginary time in the clean 2D Heisenberg model for different system sizes. (b) The same data as in (a) but plotted vs τL^{-z} ($z = D = 2$), showing how the asymptotic relaxation is governed by the Anderson tower of rotor states. In both (a) and (b) the dashed line is the magnitude of the order parameter of the Heisenberg model in the thermodynamic limit at $T = 0$. This is the value that the order parameter would relax to if the system size were infinite, and the system remained in the symmetry-broken ground state.

the order parameter (and set the effective moment of inertia, which scales as L^D [38,52]). We can confirm this intuition for the lattice model by observing that in Fig. 1(b), by rescaling the τ axis with L^2 we find that the second section of the relaxation shows scaling collapse. A consequence of this is that in the limit $L \to \infty$ the order parameter never relaxes to zero, implying that the system remains in the symmetry-broken ground state.

Next, let us discuss how to numerically extract the dynamic exponent from finite-size data. First, one must numerically determine the intersection points of $\langle m_s^z(\tau)\rangle$ with the threshold value $m_{\text{threshold}}$ required to calculate the finite-size exponent $z(L,L')$ between two system sizes. Here we choose L and $L' = 2L$, defining $z(L) \equiv z(L,2L)$. To extract τ_r we fill a window around the threshold with QMC data and then use a polynomial (or some other appropriate function) to interpolate the data and numerically find the crossing point of the interpolation and $m_{\text{threshold}}$.

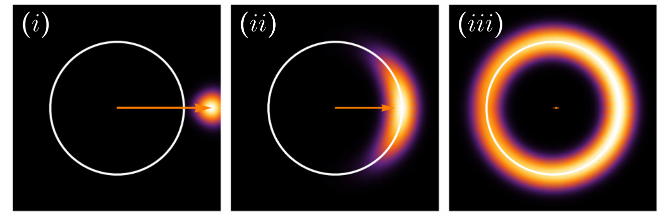

FIG. 2. Pictural representations (not based on actual data) of the probability density of the order parameter in a plane going through the origin of the O(3) space. Panels (i)–(iii) correspond to the similarly marked scaling regimes in Fig. 1(a). The radius of the white circle corresponds to the magnitude of the order parameter in the ground state, and the arrow marks the average order parameter $\langle m_s^z\rangle$. In (i) the system is close to the initial state, where the magnitude of the order parameter is larger than in the ground state. In (ii) the magnitude has decayed to its asymptotic value, but the direction of the order parameter is still close to the initial one. In (iii) the system is close to the asymptotic finite-size state with a uniformly fluctuating (not symmetry-broken) order parameter.

Next, we must derive the finite-size corrections to $z(L)$, which is dependent on the parametrization of the finite-size corrections in $\Delta(L)$. For this model it is natural to assume that $\Delta(L)$ should be an analytic function in $1/L$ because the model has no critical fluctuations. Keeping terms up to order L^{-3} in $\Delta(L)$, we find the finite-size corrections to $z(L)$ are

$$z(L) = z_\infty + \frac{c_1}{2\ln(2)}\frac{1}{L} - \frac{3(c_1^2 - 2c_2)}{8\ln(2)}\frac{1}{L^2} + \frac{7(c_1^3 - 3c_2c_1 + 3c_3)}{24\ln(2)}\frac{1}{L^3}. \tag{11}$$

The extrapolated dynamic exponents are shown as a function of $m_{\text{threshold}}$ in Fig. 3 (note that the values in Fig. 3 are correlated because $m_{\text{threshold}}$ values can be arbitrarily close to one another). The extrapolated values of z_∞ for low $m_{\text{threshold}}$ are in excellent agreement with the analytic result of $z_\infty = 2$. For higher values for $m_{\text{threshold}}$ the disagreement is natural

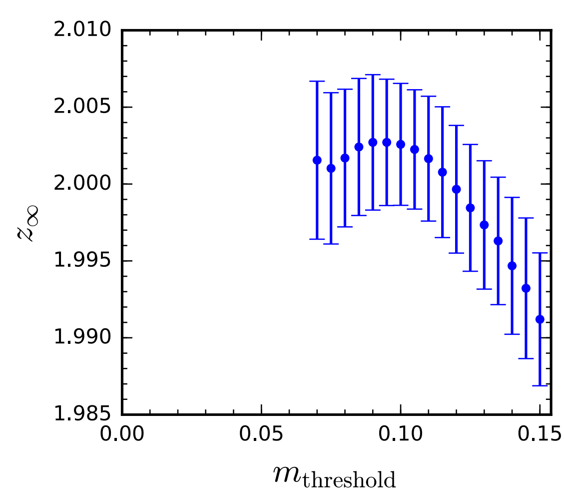

FIG. 3. Extrapolated values of the asymptotic dynamic exponent z_∞ of the clean 2D Heisenberg antiferromagnet as a function of the threshold value $m_{\text{threshold}}$ used to perform the τ-axis rescaling.

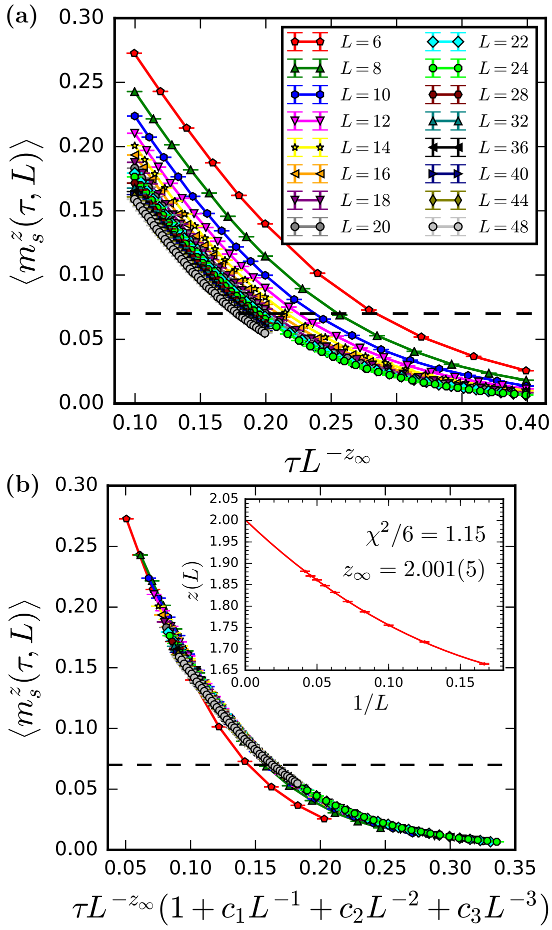

FIG. 4. Scaling collapse of $\langle m_s^z(\tau)\rangle$ in the Heisenberg model on a square lattice (a) without and (b) with finite-size corrections to the leading scaling form L^{-z_∞}. The dashed black lines denote the threshold value along which the curves are collapsed; $m_{\text{threshold}} = 0.07$. In (a), in the leading power law L^{-z_∞} the exponent is $z_\infty = 2.001$. In (b) the finite-size correction to $\Delta(L)$ is calculated from the fit to the size dependence of the exponent shown in the inset.

because at short times the many-body wave function still has an overlap with high-energy states. As the system evolves in imaginary time (as $m_{\text{threshold}}$ decreases), the overlap with these higher-energy states decays, and so their effects on the effective dynamic exponent vanish. The parameters c_i coming from the exponent flow give us the same coefficients which parametrize the finite-size corrections of $\Delta(L)$. Figure 4(a) focuses on the final relaxation time scale and more clearly shows the finite-size corrections to L^{-z}. By including the finite-size corrections calculated from the extrapolation, we find much better scaling collapse [see Fig. 4(b)].

IV. HEISENBERG ANTIFERROMAGNET ON FRACTAL CLUSTERS

The second example has the same Heisenberg interactions with nearest neighbors as the previous section, but the boundaries are no longer periodic, and spins on the sites are randomly removed from the lattice with probability $1 - p$. Models like this one have long been studied to try to understand the effects of disorder on quantum criticality [44,56–60] as well as dynamical properties of fractal geometries using spin-wave theory and other classical models [61]. At the percolation point this model has been extensively studied before, and it was found that the low-energy states responsible for spontaneous symmetry breaking have characteristics very different from those of the standard quantum rotor picture [39–41,44,62]. At the percolation point the diluted lattice can be split up into disconnected clusters which have volumes that scale as $N_c \sim L^{D_f}$, where $D_f = 91/48$ is the fractal dimension and L is a linear size of the cluster [63]. It has been conjectured that the low-energy states of a cluster are dominated by a generalization of the "dangling-spin" concept: local sublattice imbalance in a region of a given cluster [39,40] where an effective moment forms due to the inability of spins to pair up in a bipartite manner. On a Bethe lattice geometry the same phenomenon was studied using the DMRG method [41]. In this study it was shown explicitly that there exists a set of low-lying quasidegenerate (QD) eigenstates which remain separated from the higher-energy eigenstates by a finite-size gap Δ_{QD}, which goes to zero slower than the spacing between the QD states. It was conjectured that these QD states decouple from the bulk because they are made up of power-law localized magnetic moments which interact with each other across the cluster, as previously deduced based on scaling behaviors of quantities probing the low-energy excitations indirectly [39,40]. For this reason, diluted Heisenberg models have a larger dynamic exponent than predicted by the quantum rotor picture [39–41,62].

Beyond the interesting physics of this model, the disorder should prove a more robust test of our scaling hypothesis and method for extracting the dynamic exponent. The major difference between this model and the last is the type of finite-size corrections we see. In the unadulterated 2D case, the model is very far away from any sort of critical behavior, and so the corrections are analytic in L^{-1}, but here we cannot assume this as there are fluctuations driven by the classical percolation threshold [44]. However, since we are interested only in extracting the dynamic exponent, it is perfectly reasonable to parametrize the finite-size corrections to be analytic in N^{-1}, where N is the number of sites making up a cluster.

To perform the dilution averaging we employ a procedure similar to what is outlined in Ref. [44]. Each cluster is constructed with a fixed number of sites $N_c = L^{D_f}$, where we round up to an even integer to ensure that the ground state can have total $S = 0$. The finite-size scaling of the low-energy gap is implemented in the following form:

$$\Delta(N) = N^{-z_\infty/D_f}(1 + c_1 N^{-1} + c_2 N^{-2} + \cdots). \tag{12}$$

The finite-size flow of the effective dynamic exponents is calculated between system sizes of length L and $2L$, which implies $N' = 2^{D_f} N$ for the cluster sizes. Keeping terms up to order N^{-2} in finite-size corrections to $\Delta(N)$, we obtain the following expansion for the finite-size effective dynamic

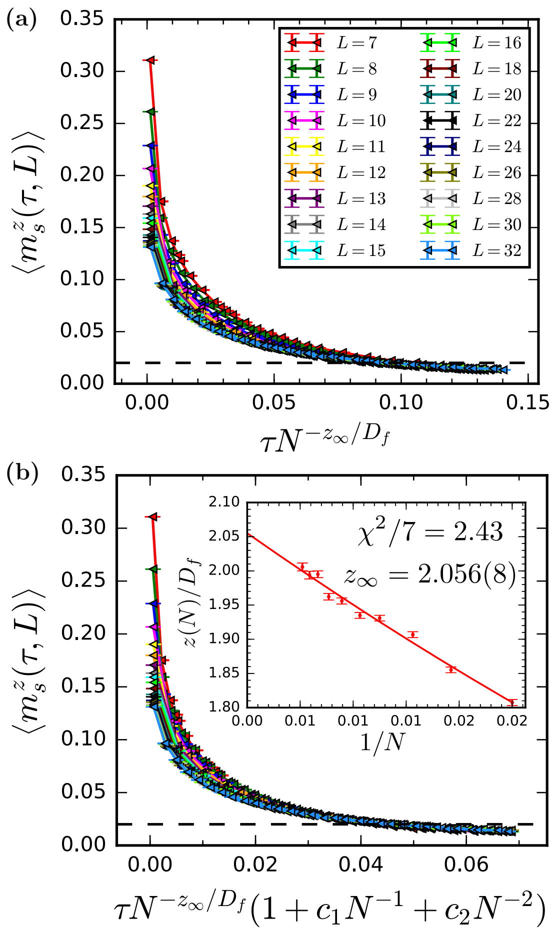

FIG. 5. Finite-size scaling analysis of $\langle m_s^z(\tau)\rangle$ in the Heisenberg model on a percolating cluster (averaged over dilution realizations). The black dashed line denotes the threshold value along which the curves are collapsed; $m_{\text{threshold}} = 0.02$. (a) The data collapse with the leading behavior N^{-z_∞/D_f} used for rescaling the x axis, with $z_\infty/D_f = 2.065$. (b) The scaling collapse including the finite-size correction to $\Delta(N)$ corresponding to the fit of the finite-size flow shown in the inset.

exponent $z(N)$:

$$\frac{z(N)}{D_f} = \frac{z_\infty}{D_f} + \frac{c_1(2^{D_f}-1)}{2^{D_f}\ln(2^{D_f})}\frac{1}{N} - \frac{3(2^{2D_f}-1)(c_1^2-2c_2)}{2^{2D_f}\ln(2^{D_f})}\frac{1}{N^2}. \tag{13}$$

The results of a data-collapse analysis both with and without the scaling corrections are shown in Fig. 5.

For our lowest value of $m_{\text{threshold}} = 0.02$, $z_\infty/D_f = 2.056(8)$ or $z_\infty = 3.90(1)$, slightly larger than what was found in previous studies [39,40]. Although we may have introduced some systematic error by assuming the finite-size corrections decay as $1/N$, the inset in Fig. 5(b) shows that for the largest system size ($N = 714$), $z(N)/D_f \geqslant 2$. Because our system sizes are comparable to those in previous studies, we know that this is not an issue of finite-size effects. We also know that in imaginary-time evolution, the weights coming from an eigenstate $|n\rangle$ relax on a time scale of $\tau_n = 1/(\epsilon_n - \epsilon_0)$, meaning that higher-energy states always decay faster than low-energy states and therefore the effective dynamic exponents must be monotonically increasing as $m_{\text{threshold}} \to 0$. This is consistent with results in the previous section and with the threshold dependence of the extrapolated dynamic exponent shown in Fig. 6.

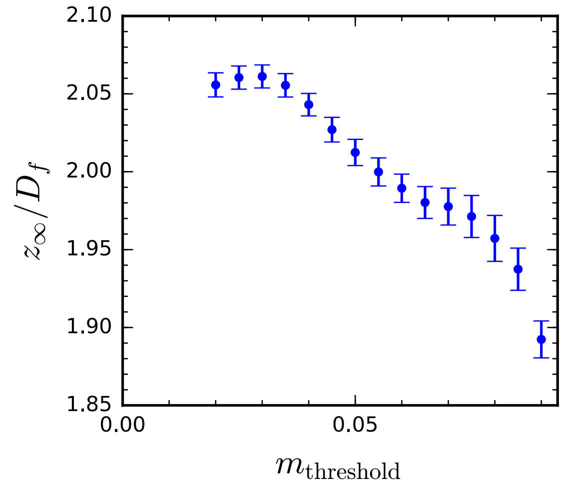

FIG. 6. Extrapolated values of z_∞ averaged over the dilution realization for the site-diluted Heisenberg antiferromagnet as a function of the threshold value $m_{\text{threshold}}$ used to perform the τ-axis rescaling.

V. CONCLUSION

In summary we have shown that the relaxation of the order parameter in imaginary time can be used to quantitatively extract low-energy properties of a given model. In particular, we have developed a scaling method which allows one to extract the dynamic exponent by performing scaling collapse of the order parameter along the imaginary-time axis. The imaginary-time evolution of the order parameter in 2D Heisenberg antiferromagnets was used as a test case to show that one can extract the correct dynamic exponent, which in this case is related to the Anderson tower of quantum rotor states. We also studied the relaxation of the order parameter of the corresponding site-diluted Heisenberg antiferromagnet at its percolation threshold and found that the scaling theory gives a dynamic exponent even larger than that seen in previous studies, $z = 3.90$ versus $z \approx 3.7$ from Refs. [39,40]. These results conform with the notion that there is a set of low-energy states due to quasilocalized moments: dangling spins and their generalizations to larger regions of local sublattice imbalance [39,40].

As there are very clear numerical results that the ground state of the Heisenberg model on the percolating cluster does, indeed, have long-range order [44], there is still an open question of whether there is a quantum rotor tower of states in these clusters, which presumably should be required for spontaneous breaking of the spin-rotation symmetry in the thermodynamic limit [38,42]. If they do exist, they would have relaxation times that would scale as L^{D_f} according to the quantum rotor picture; however, our method would not be able to isolate these states directly as it can extract only an effective dynamic exponent originating from the mixing of low- and high-energy states at short times. The fact that we see a dynamic exponent with significant flow with a threshold value of the mean order parameter in the system, much larger than in the unadulterated system, may, in principle, be an indication of the rotor states. However, the density of the rotor states should be much lower than the low-energy states arising from the quasilocalized moments. The drift in the exponent may therefore instead be related to a slowly changing dynamic exponent of these quasilocalized states as one goes to higher energies in their tower. We believe that this is the more likely scenario, with rotor states existing in the bulk of the cluster but not contributing significantly to the low-energy dynamics because of their much higher dynamic exponent and much lower density of states.

In this work we have studied only the spatially averaged order parameter, but in the case of the percolating clusters it could be useful to look at the local order as a function of imaginary time in a spirit similar to that of Refs. [39,40]. One would expect that if the localized spins are, indeed, decoupled from the bulk, this would manifest itself as very different relaxation times between the localized moments and the bulk. One would even hope to see that the bulk relaxes to zero on time scales $\tau \sim L^{D_f}$, while the decoupled moments would relax on time scales of $L^{3.90}$.

The QMC methods used here to simulate imaginary time can be generalized to higher-spin representations which, along with other methods, would give a more complete picture of the low-energy excitations of the higher-spin versions of the Heisenberg antiferromagnets on percolating clusters. Finally, we have focused extensively on Heisenberg antiferromagnets, but this method of determining the dynamic exponent can be applied to any model which can be simulated with QMC, for example, long-range interacting transverse-field Ising chains, which have recently been studied in other contexts for these interesting critical and dynamic properties [64–67].

ACKNOWLEDGMENTS

We would like to thank H. Changlani, A. Iaizzi, P. Patil, and A. Polkovnikov for useful discussions. The computation was performed on the Shared Computing Cluster administered by Boston University's Research Computing Services. This research was supported by the NSF under Grant No. DMR-1410126.

[1] M. Paillard, X. Marie, P. Renucci, T. Amand, A. Jbeli, and J. M. Gérard, Phys. Rev. Lett. **86**, 1634 (2001).
[2] S. Kaiser, C. R. Hunt, D. Nicoletti, W. Hu, I. Gierz, H. Y. Liu, M. Le Tacon, T. Loew, D. Haug, B. Keimer, and A. Cavalleri, Phys. Rev. B **89**, 184516 (2014).
[3] S. Loth, M. Etzkorn, C. P. Lutz, D. M. Eigler, and A. J. Heinrich, Science **329**, 1628 (2010).
[4] I. Bloch, Nat. Phys. **1**, 23 (2005).
[5] L. E. Sadler, J. M. Higbie, S. R. Leslie, M. Vengalattore, and D. M. Stamper-Kurn, Nature (London) **443**, 312 (2006).
[6] S. Ritter, A. Öttl, T. Donner, T. Bourdel, M. Köhl, and T. Esslinger, Phys. Rev. Lett. **98**, 090402 (2007).
[7] S. Trotzky, Y.-A. Chen, A. Flesch, I. P. McCulloch, U. Schollwck, J. Eisert, and I. Bloch, Nat. Phys. **8**, 325 (2012).
[8] M. Schreiber, S. S. Hodgman, P. Bordia, H. P. Lüschen, M. H. Fischer, R. Vosk, E. Altman, U. Schneider, and I. Bloch, Science **349**, 842 (2015).
[9] R. Nandkishore and D. A. Huse, Annu. Rev. Condens. Matter Phys. **6**, 15 (2015).
[10] R. Vosk and E. Altman, Phys. Rev. Lett. **110**, 067204 (2013).
[11] A. Pal and D. A. Huse, Phys. Rev. B **82**, 174411 (2010).
[12] V. Oganesyan and D. A. Huse, Phys. Rev. B **75**, 155111 (2007).
[13] J. Z. Imbrie, J. Stat. Phys. **163**, 998 (2016).
[14] I. V. Gornyi, A. D. Mirlin, and D. G. Polyakov, Phys. Rev. Lett. **95**, 206603 (2005).
[15] D. M. Baskoa, I. L. Aleiner, and B. L. Altshuler, Ann. Phys. (NY) **321**, 1126 (2006).
[16] A. J. Daley, C. Kollath, U. Schollwck, and G. Vidal, J. Stat. Mech. (2004) P04005.
[17] U. Schollwck, Rev. Mod. Phys. **77**, 259 (2005).
[18] U. Schollwck, Ann. Phys. (NY) **326**, 96 (2011).
[19] M. Jarrell and J. E. Gubernatis, Phys. Rep. **269**, 133 (1996).
[20] C. De Grandi, A. Polkovnikov, and A. W. Sandvik, Phys. Rev. B **84**, 224303 (2011).
[21] C. D. Grandi, A. Polkovnikov, and A. W. Sandvik, J. Phys. Condens. Matter **25**, 404216 (2013).
[22] C.-W. Liu, A. Polkovnikov, and A. W. Sandvik, Phys. Rev. B **87**, 174302 (2013).
[23] T. W. B. Kibble, J. Phys. A **9**, 1387 (1976).
[24] W. H. Zurek, Nature (London) **317**, 505 (1985).
[25] A. Polkovnikov, Phys. Rev. B **72**, 161201(R) (2005).
[26] W. H. Zurek, U. Dorner, and P. Zoller, Phys. Rev. Lett. **95**, 105701 (2005).
[27] J. Dziarmaga, Phys. Rev. Lett. **95**, 245701 (2005).
[28] F. Zhong and Z. Xu, Phys. Rev. B **71**, 132402 (2005).
[29] A. Chandran, A. Erez, S. S. Gubser, and S. L. Sondhi, Phys. Rev. B **86**, 064304 (2012).
[30] C.-W. Liu, A. Polkovnikov, and A. W. Sandvik, Phys. Rev. B **89**, 054307 (2014).
[31] M. Kolodrubetz, Phys. Rev. B **89**, 045107 (2014).
[32] S. Yin, P. Mai, and F. Zhong, Phys. Rev. B **89**, 144115 (2014).
[33] S. Zhang, S. Yin, and F. Zhong, Phys. Rev. E **90**, 042104 (2014).
[34] Y.-R. Shu, S. Yin, and D.-X. Yao, arXiv:1705.05931.
[35] A. Chiocchetta, A. Gambassi, S. Diehl, and J. Marino, Phys. Rev. B **94**, 174301 (2016).
[36] W. Liu and U. C. Tuber, J. Phys. A **49**, 434001 (2016).
[37] H. Shao, W. Guo, and A. W. Sandvik, Phys. Rev. B **91**, 094426 (2015).
[38] P. W. Anderson, Phys. Rev. **86**, 694 (1952).
[39] L. Wang and A. W. Sandvik, Phys. Rev. Lett. **97**, 117204 (2006).
[40] L. Wang and A. W. Sandvik, Phys. Rev. B **81**, 054417 (2010).
[41] S. Ghosh, H. J. Changlani, and C. L. Henley, Phys. Rev. B **92**, 064401 (2015).
[42] J. Goldstone, A. Salam, and S. Weinberg, Phys. Rev. **127**, 965 (1962).

[43] T. Vojta and J. Schmalian, Phys. Rev. Lett. **95**, 237206 (2005).
[44] A. W. Sandvik, Phys. Rev. B **66**, 024418 (2002).
[45] D. S. Fisher, Phys. Rev. B **39**, 11783 (1989).
[46] P. Nightingale, J. Appl. Phys. **53**, 7927 (1982).
[47] E. Brezin, J. Phys. **43**, 15 (1982).
[48] L. D. S. B. Derrida, J. Phys. **43**, 475 (1983).
[49] M. Luck, Phys. Rev. B **31**, 3069 (1985).
[50] H. Neuberger and T. Ziman, Phys. Rev. B **39**, 2608 (1989).
[51] P. Hasenfratz and F. Niedermayer, Z. Phys. B **92**, 91 (1993).
[52] A. W. Sandvik, *Lectures on the Physics of Strongly Correlated Systems XIV: Fourteenth Training Course in the Physics of Strongly Correlated Systems*, AIP Conf. Proc. No. 1297 (AIP, New York, 2010), p. 135.
[53] A. W. Sandvik and H. G. Evertz, Phys. Rev. B **82**, 024407 (2010).
[54] C. Lavalle, S. Sorella, and A. Parola, Phys. Rev. Lett. **80**, 1746 (1998).
[55] A. W. Sandvik, Phys. Rev. B **56**, 11678 (1997).
[56] S. J. Lewis and R. B. Stinchcombe, Phys. Rev. Lett. **52**, 1021 (1984).
[57] E. Manousakis, Phys. Rev. B **45**, R7570 (1992).
[58] J. Behre and S. Miyashita, J. Phys. A **25**, 4745 (1992).
[59] C. Yasuda and A. Oguchi, J. Phys. Soc. Jpn. **66**, 2836 (1997).
[60] Y.-C. Chen and A. H. C. Neto, Phys. Rev. B **61**, R3772 (2000).
[61] T. Nakayama and K. Yakubo, *Fractal Concepts in Condensed Matter Physics* (Springer, Berlin, 2003).
[62] H. J. Changlani, S. Ghosh, S. Pujari, and C. L. Henley, Phys. Rev. Lett. **111**, 157201 (2013).
[63] D. Stauffer and A. Aharony, *Introduction to Percolation Theory* (CRC Press, Boca Raton, 1994).
[64] A. W. Sandvik, Phys. Rev. E **68**, 056701 (2003).
[65] T. Koffel, M. Lewenstein, and L. Tagliacozzo, Phys. Rev. Lett. **109**, 267203 (2012).
[66] D. Vodola, L. Lepori, E. Ercolessi, and G. Pupillo, New. J. Phys. **18**, 015001 (2016).
[67] D. Jaschke, K. Maeda, J. Whalen, M. Wall, and L. Carr, New. J. Phys. **19**, 033032 (2017).